Electronic Supplementary Material (ESI) for Soft Matter.
This journal is © The Royal Society of Chemistry 2019

Soft Matter

ARTICLE TYPE

Cite this: DOI: 00.0000/xxxxxxxxxx

PDMS Polymerized High Internal Phase Emulsions (polyHIPEs) with Closed-cell, Aqueous-filled Microcavities - Supplementary Information

Amrita Kataruka, Shelby B. Hutchens*

1 Viscosity Determination

The dual asymmetric mixer consists of a 2.3 cm radius cup (r_{cup}) rotating about its central axis while being spun about an approximately normally oriented external axis on a ~ 6.2 cm arm (r_{arm}). For 1500 to 3500 rpm mixing speeds (ω_c, (cycles/time)), the approximate shear rate, $\dot{\gamma}$, scales with the velocity of the outer edge of the cup ($2\pi r_{\text{cup}}\omega_c$) divided by the cup radius, or $\approx 160 - 370$ Hz. Viscosity approaches a plateau at shear rates around 300 Hz. To provide a means of systematic comparison of the flow behavior of all components at the high shear rates estimated for the DAC mixer, we fit a power law to the rheometric viscosity versus shear-rate data. Fig. S1 shows a representative example. The plateau viscosity obtained from the curve fit, as shear rate approaches infinity, is taken to be the viscosity of the component.

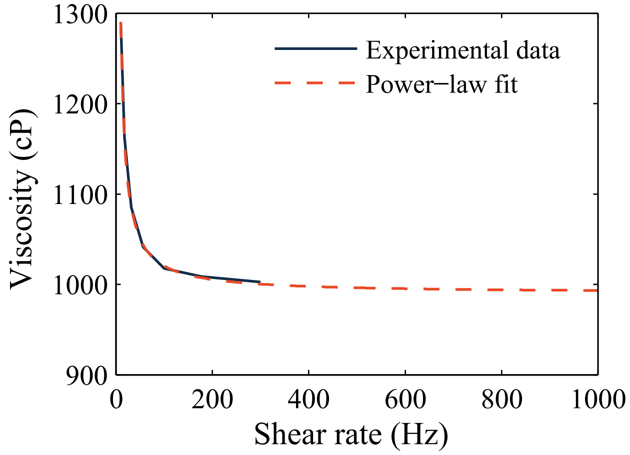

Fig. S1 Viscosity as a function of shear rate for a representative continuous phase sample (PDMS + hexane + SNP). The dashed line shows the power law curve fitting up to an extended shear rate of 1000 Hz.

2 Image analysis: Emulsion

Bright field optical images of uncured emulsions are obtained in a ZEISS inverted microscope. Figure S2 illustrates a sample micrograph (a), followed by the image at key stages in the analysis process (b-d). First, the circular edges of the droplets are found using a built-in function (*Process - Find edges*) in ImageJ (Fig. S2(b)). The image is then converted to 8-bit before carrying out a threshold segmentation (Fig. S2(c)). We analyze droplet size using an open-source ImageJ plug-in ('Hough circle transform'). This plug-in detects the circles in the image and returns their radii. Fig. S2(d) shows an overlay of the detected circles on the color inverted segmented image. We find that the performance of the plug-in is sensitive to image noise in the image and thus requires good image quality and robust segmentation. Several micrographs are characterized in this way until >300 droplets have been detected and quantified.

3 Image analysis: polyHIPE

Volume fraction & cavity size determination: We calculate the volume fraction of the aqueous phase by analyzing 5 consecutive images from the microCT stack in ImageJ. Cavity size distributions are obtained through particle analysis on a single image (approx. 150 droplets). The analysis procedure for both scenarios is illustrated in Fig. S3. A single, cropped microCT image from the stack (Fig. S3(a)) is first enhanced by subtracting the background (Fig. S3(b)). After segmenting the enhanced image using the 'Robust Automatic Threshold Selection' plug-in (Fig. S3(c)), particle analysis is performed. The particle analysis returns the major and minor axes of the cavities by fitting an ellipse (Fig. S3(d)). For the purpose of comparison, we estimate the size of the cavities by equating the area of the fitted ellipse to that of an equivalent circle. Fig. S3(e) shows an overlay of the ellipses determined in this way on the actual image, providing a visual validation of the process. Gradient characterization repeats this process for every 100th slice, starting from the 50th slice to the 950th slice.

Particle analysis also returns the area fraction of the black portion of the segmented image, corresponding to the cavity area fraction. Total cavity volume is simply a sum of each the area fractions from five slices multiplied by the product of the total image area, A, and the slice thickness, t (equivalent to the rectangle integration rule). Dividing the total cavity volume by the total image volume ($5At$) yields the volume fraction, which is equivalent to the average area fraction over the five image.

Wall thickness: MicroCT image quality was determined to be

University of Illinois at Urbana Champaign, Urbana, United States.
Tel: +1(217)300-0412; E-mail: hutchs@illinois.edu

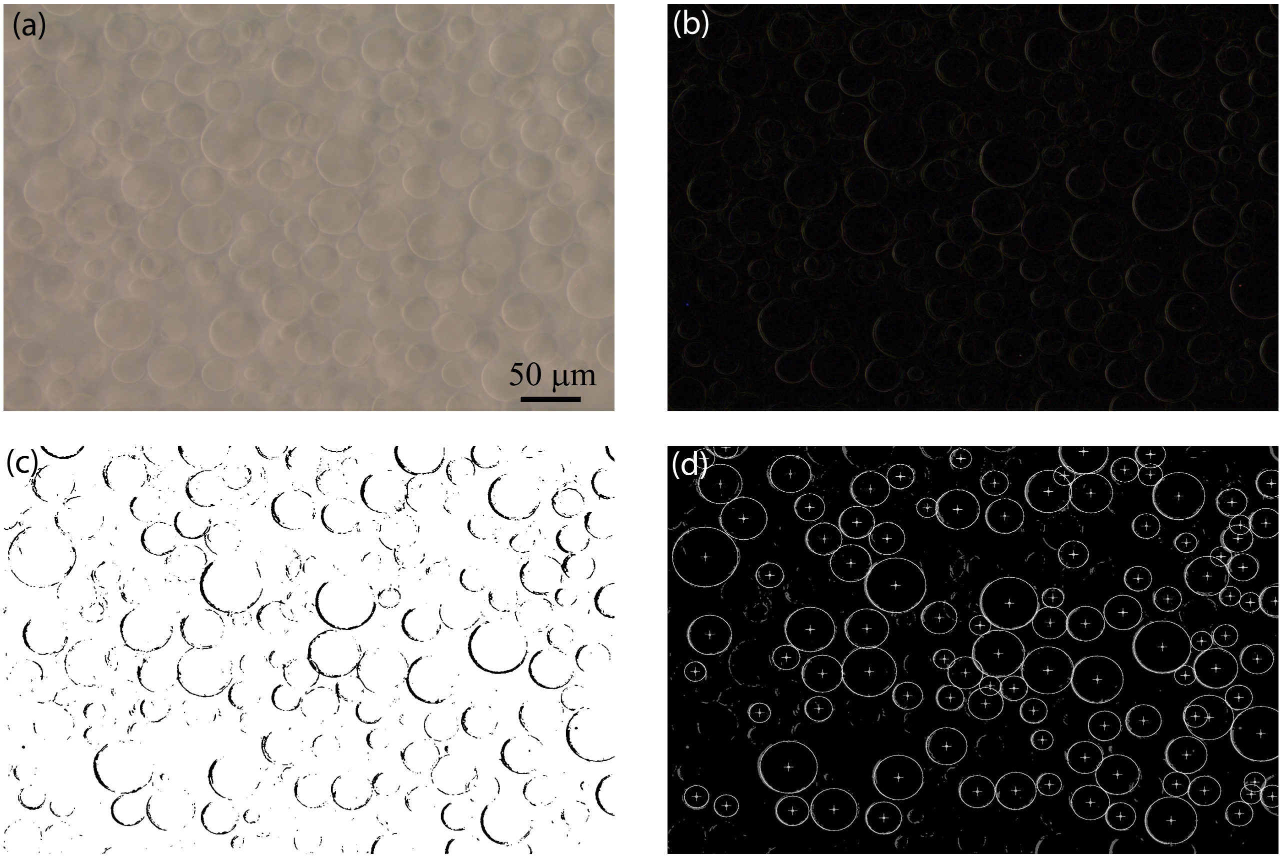

Fig. S2 Emulsion image analysis procedure.(a) An typical optical micrograph from an uncured LIPE; (b) The image after edge detection; (c) A segmented image using the ImageJ's built-in threshold function; (d) An overlay of circles detected by the 'Hough circle transform' plug-in on the segmented, inverted image.

insufficient for robust, automated wall thickness measurement. Instead, 30 randomly computer-generated points are selected on a scanning electron micrograph (SEM) of a cross-section of the samples. The cavity wall closest to each point is manually measured in ImageJ.

4 Probability density functions

Raw droplet and cavity size distribution data consists of discrete values. Histograms generated from this data make direct comparison difficult and trends less visually apparent. To facilitate understanding, we fit each data set to either or normal (N) or lognormal (LN) probability density function (pdf). The best fitting distribution for the data is selected based on a weighted ranking of three goodness of fit tests (Kolmogorov-Smirnov, Anderson-Darling, and Chi-Squared) in the software EasyFit. We find all data to be well-described by either N or LN distributions. An example pdf fit is shown in Fig. S4. Histograms are generated for the droplet/cavity size measurements using *n* equally spaced bins, determined via Sturge's rule. For the example shown, the lognormal distribution is a better fit.

5 Emulsion and Droplet control

5.0.1 Water Content Limitations

We attribute emulsification limitations to two key parameters known to govern droplet break-up in Newtonian fluids:[1] the viscosity ratio between the components, $\lambda = \eta_d/\eta_c$, and the capillary number,

$$\mathrm{Ca} = \frac{\tau}{2\sigma/d}, \tag{1}$$

which accounts for the relative contributions from shear stress, τ, leading to droplet deformation, and the Laplace pressure, preventing break-up. Here σ is the surface energy and d is the droplet diameter.

The phenomenon of increasing maximum dispersed phase content with increasing viscosity ratio in the regime we test here may be consistent with theories of droplet break up for Newtonian fluids.[1,2] We limit discussion to droplet breakup under shear mixing given its predominance in the DAC mixer used. For single, non-interacting droplets, Grace[1] found that droplet breakup occurs above a critical value for the capillary number ($\mathrm{Ca}_{\mathrm{crit}}$) and that this critical value is a function of λ. Figure S5 illustrates the Grace curve. Above a viscosity ratio of 4, breakup does not occur, while for a given Ca, there exists a minimum value of λ for breakup as well. Although the Grace curve was determined for single droplet breakup, Jansen *et al.*[3] showed that in con-

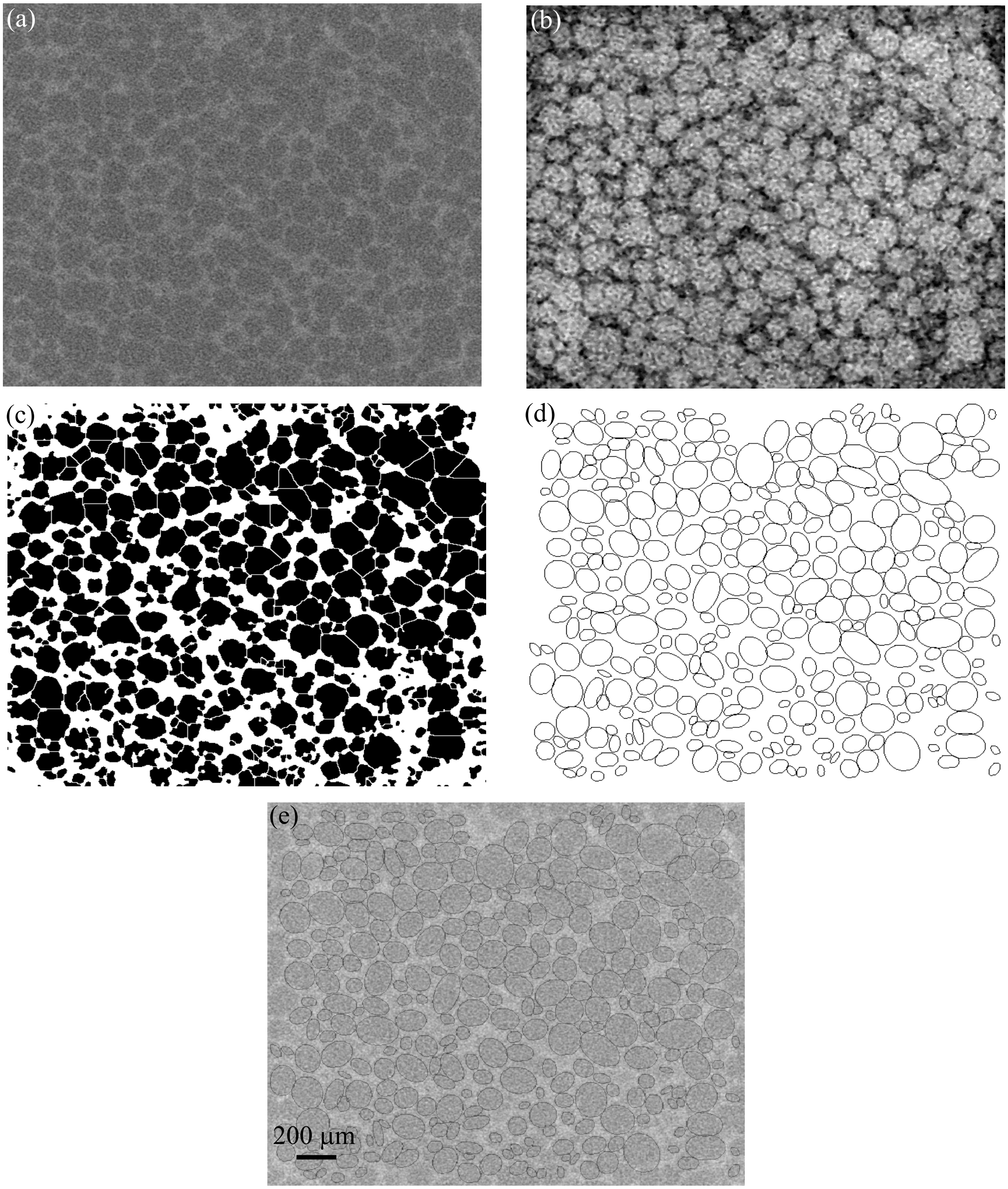

Fig. S3 PolyHIPE image analysis procedure.(a) A single, representative microCT stack image; (b) The image after being enhanced by subtracting the background; (c) The image after segmentation carried out using the 'Robust Automatic Threshold Selection' plug-in in ImageJ; (d) The result of particle analysis on the segmented image in the form of elliptical fits; (e) An overlay of the identified cavities (ellipses) on the original image.

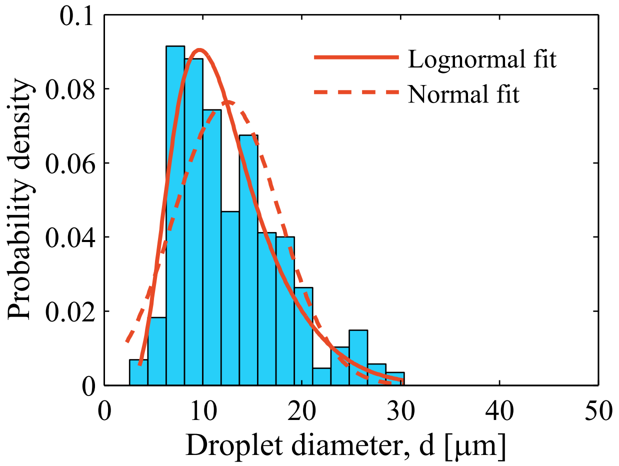

Fig. S4 Lognormal (solid line) and normal (dashed line) probability distribution fits superimposed on the histogram of droplet diameter for a representative data set.

centrated emulsions, the curve applies so long as the continuous phase viscosity is replaced by the average emulsion viscosity, η_e, resulting in a modified viscosity ratio, $\lambda^* = \eta_c/\eta_e$.[§] Thus we use the Grace curve to qualitatively interpret the emulsification limit trends we observe.

The experimentally-observed trend may be rationalized as follows. For DAC mixing, we consider the centrifugal forces acting to pull the fluid contents toward the bottom of the mixing cup due to rotation around an axis external to the cup and those forcing the fluid to flow up the cup walls via rotation about the cup's axis of symmetry. Applying the principle of super position, treating these three tensile stresses as the principal stresses, and calculating the maximum shear stress, τ, (located at the top and center of the cup) under the assumption that the fluid maintains an approximately cylindrical shape within the cup yields

$$\tau \approx \frac{\rho \omega^2}{2} r_\mathrm{cup} r_\mathrm{arm} \tag{2}$$

where ρ is the mass density, ω is the angular velocity (rad/s) of both rotations, r_cup is the radius of the mixing cup, and r_arm is the length of the rotating arm within the mixer. For the 2.3 cm radius cup rotating on a 6.2 cm arm at 3500 rpm, the shear stress is approximately 100 kPa ($\rho \approx 1000$ kg/m^3). It follows that for an estimated $d \approx 25$ μm (Fig. 3(b)) and $\sigma \approx 40$ mN/m (water-PDMS interface), the capillary number applied by the mixer is on the order of 30. Figure S5 illustrates this state within the Grace curve for component viscosity ratios at the 3 wt$_\mathrm{o}$% SNP concentration for hexane content at the lowest and highest amounts tested (0 and 64 wt$_\mathrm{o}$%, $\lambda = 0.0005$ and 0.042, blue and medium orange circles, respectively). We use this order of magnitude starting point to demonstrate the experimentally observed trend.

As more aqueous phase is added, the modified viscosity ratio, λ^*, deviates further (decreases) relative to the component viscosity ratio, translating the state of the system horizontally, in the direction of the corresponding arrows. As Fig. S5 illustrates, the higher the starting component viscosity ratio, the longer the emulsion remains within the droplet breakup window. Lower starting viscosity ratios thus reach their maximum aqueous phase content earlier, consistent with every SNP concentration shown in Fig. 2(a). The effect of SNP concentration on maximum aqueous phase content may be similarly described using Fig. S5. Taking the 3 wt$_\mathrm{o}$% SNP, 64 wt$_\mathrm{o}$% hexane point (medium orange circle) as the reference, an increase in SNP for a sample with identical component ratio viscosity will correspond to more nanoparticles at the droplet surfaces, thereby lowering the surface energy. This lower surface energy increases the capillary number applied by the mixer (dark orange circle). As the droplet breakup window enlarges at higher Ca, we expect the addition of more nanoparticles to correspond to an increase in the maximum aqueous phase content for similar viscosity ratio. The opposite is true for decreased SNP concentration (light orange circle). This result is also consistent with experimental observation, Fig. 2(a). We note that for the viscosity ratios observed, the 2 wt$_\mathrm{o}$% formulations never reach the HIPE state (only 71 wt$_\mathrm{e}$%). The significantly lower maximum aqueous phase content at this SNP concentration may also be affected by insufficient surface coverage leading to droplet coalescence. Effects of droplet coalescence are not captured by the Grace curve.

5.0.2 Droplet Tuning

Figure S6 exemplifies the saturation behavior associated with increasing emulsion stabilizer concentration. Distributions at the higher concentrations, 3 and 4 wt$_\mathrm{o}$%, do not differ significantly over the range of mixing speeds tested (23 wt$_\mathrm{e}$%).

We perform a few parameter checks to validate the trends reported in Fig. 3. To determine the lower bound of mean droplet diameter possible through manipulation of both viscosity ratio and mixing speed, we characterize a sample at a low hexane content value (20 wt$_\mathrm{o}$%, $\lambda = 1.6 \times 10^{-3}$) and the highest mixing speed (3500 rpm). We achieve $\bar{d} = 6.95$ μm and S = 0.88 with this combination of composition and processing parameters (23 wt$_\mathrm{e}$% aqueous phase). As shown in Figure S7, the same sample ($\lambda = 1.6 \times 10^{-3}$) mixed at 2000 rpm results in $\bar{d} = 11$ μm and S = 1.04, approximately doubling in size, in line with Fig. 3(b). We also characterized a sample at 50 wt$_\mathrm{o}$% hexane content ($\lambda = 4.5 \times 10^{-3}$) mixed at the highest mixing speed (3500 rpm). This sample produced an even larger average droplet diameter $\bar{d} = 23$ μm and S = 1.00. This trend is predicted by interpolation of results in Fig. 3. Therefore, by careful selection of processing parameters, droplets of desired size can be produced.

Notes and references

1 H. P. Grace, *Chem. Eng. Commun.*, 1982, **14**, 225–277.
2 R. A. Debruijn, *PhD thesis*, 1991.
3 K. Jansen, W. Agterof and J. Mellema, *J. Rheol.*, 2001, **45**, 227–236.

[§] Emulsion viscosity, η_e, replaces η_c in both the calculation of λ and the determination of the critical capillary number such that $\mathrm{Ca_{crit}} = \eta_c \dot{\gamma}/(2\sigma/d)$ becomes $\mathrm{Ca^*_{crit}} = \eta_e \dot{\gamma}/(2\sigma/d)$. $\dot{\gamma}$ is the shear strain rate.

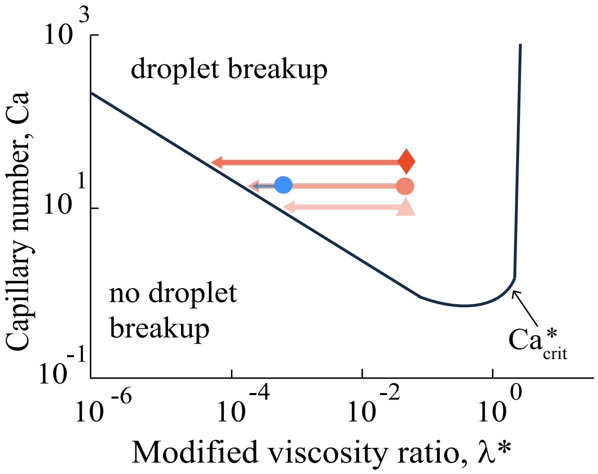

Fig. S5 A schematic illustration of the Grace curve showing the dependence of droplet breakup on capillary number and viscosity ratio.

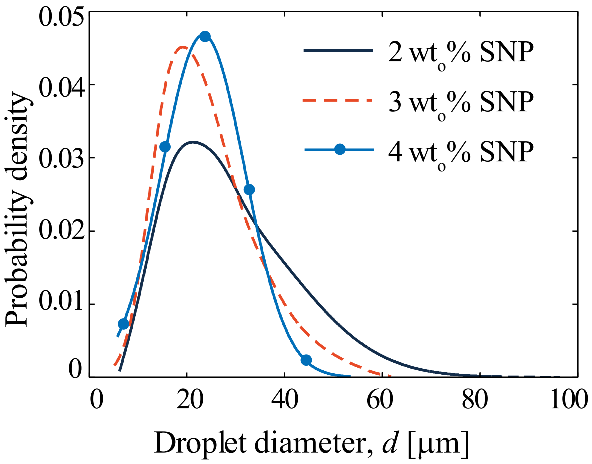

Fig. S6 Probability densities for droplet diameters produced using 2 (dark blue-solid), 3 (red-dash), and 4 (light blue-solid with circles) wt_o% SNP concentrations mixed at 3500 rpm follow lognormal, lognormal, and normal distributions, respectively.

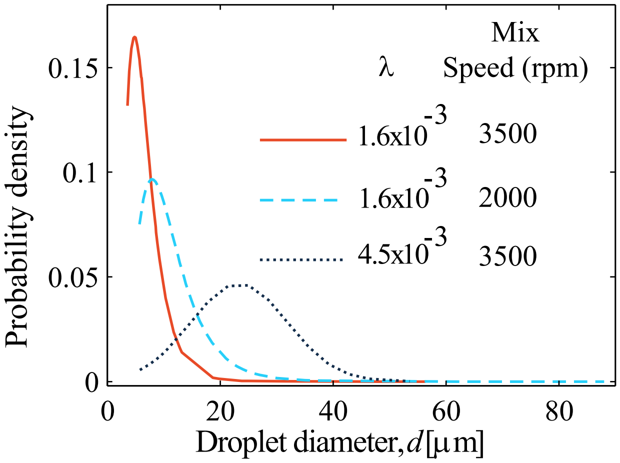

Fig. S7 Probability densities for droplet size control validation samples. The combined effect of high mixing speed (3500 rpm) and low viscosity ratio (1.6×10^{-3}) generate droplets with a mean diameter of less than 10 μm (solid, red curve, LN distribution). The teal dashed line ($\lambda = 1.6 \times 10^{-3}$; 2000 rpm, LN distribution) has a larger mean and span because it was mixed at a lower speed. Similarly, the dark blue dotted line ($\lambda = 4.5 \times 10^{-3}$; 3500 rpm, N distribution) has the largest span and mean droplet diameter due to its higher viscosity ratio.